# DESIGN OF AN INTENSE MUON SOURCE WITH A CARBON AND MERCURY TARGET

Diktys Stratakis, J. Scott Berg, BNL*, Upton, NY 11973, USA
David Neuffer, Fermilab†, Batavia, IL, USA
Xiaoping Ding, University of California, Los Angeles, CA, USA

*Abstract*

In high-intensity sources, muons are produced by firing high energy protons onto a target to produce pions. The pions decay to muons which are captured and accelerated. In the present study, we examine the performance of the channel for two different target scenarios: one based on liquid mercury and another one based on a solid carbon target. We produce distributions with the two different target materials and discuss differences in particle spectrum near the sources. We then propagate the distributions through our capture system and compare the full system performance for the two target types.

## INTRODUCTION

In this paper we will first discuss the particle distributions created from a C target and a Hg target. We will describe our muon capture and initial cooling scenario, and then present results of simulation of that front end system.

## PARTICLE DISTRIBUTIONS

We produce particle distributions from mercury and carbon targets under similar conditions. A proton bunch hits a target, with the relevant parameters described in Table 1. The target is in a field that peaks near 20 T at the center of the beam-target crossing, and tapers down to 2 T just under 5 m downstream, and continues at that field downstream from that point. The solenoids that produce this field are described in Table 2; the choice of this field profile was based on [1]. A beam pipe with an inner radius of 13 cm surrounds the target and extends downstream to 85 cm from the beam-target crossing point. Downstream from there, the beam pipe has an inner radius of 23 cm. Particle production computations were performed using MARS15(2014) [2, 3].

We found that the choice of event generator parameters for nuclear inelastic interactions had a significant impact on particle production, as shown in Fig. 1. In contrast to [4, 5], but like [6], these studies use IQGSM=1, the current MARS15(2014) default [3]. Pion production per unit of proton power in mercury is notably higher than in carbon for lower pion energies, but the production rapidly becomes closer above 250 MeV (Figs. 2 and 3). The differences are much larger for negative than for positive pions. Thus the particle capture system should be optimized differently for a mercury than for a carbon target due to the lower-energy spectrum in mercury. Furthermore, the difference in the spectral shape between positive and negative pions in mercury requires that the optimal capture parameters for positive and negative particles will be different, and some application-

Table 1: Parameters of the target and incident proton beam. Carbon target parameters are taken from [6], without the dump, with the target radius increased to 10 mm, and a corresponding increase in the proton beam size. For mercury, the target, proton beam, and solenoid axis lie in the same plane at the crossing point, with the proton beam to the outside. The optimization process for obtaining the target geometry is described in [4].

| **Material** | **C** | **Hg [5]** |
|---|---|---|
| Target Radius (mm) | 10.00 | 4.04 |
| RMS Beam Size (mm) | 2.5 | 1.212 |
| Target Tilt (mrad) | 65 | 127 |
| Crossing Angle (mrad) | 0 | 20.6 |
| Proton Energy (GeV) | 6.75 | 8 |
| Geometric Emittance (μm) | 5 | 0 |

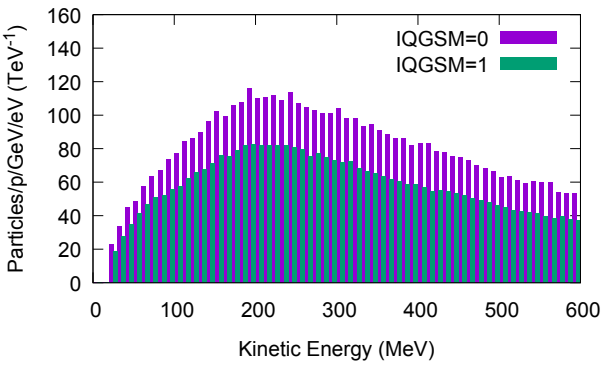


Figure 1: Spectrum of positive pions from carbon, 2 m downstream from the beam-target crossing, for different values of IQGSM in MARS15(2014) [3]: IQGSM=0 is the default value used in older MARS versions, and was used in [4, 5]; IQGSM=1 is the current default value in MARS and was used in [6] and elsewhere in this study. Values are divided by proton beam energy in GeV and histogram bin width.

* This manuscript has been authored by employees of Brookhaven Science Associates, LLC under Contract No. DE-SC0012704 with the U.S. Department of Energy. The United States Government retains a non-exclusive, paid-up, irrevocable, world-wide license to publish or reproduce the published form of this manuscript, or allow others to do so, for United States Government purposes.
† Operated by Fermi Research Alliance, LLC under Contract No. DE-AC02-07CH11359 with the United States Department of Energy.

Table 2: Solenoid Coil Geometries and Currents [7]

| **Inner Radius (m)** | **Outer Radius (m)** | **Front Position (m)** | **End Position (m)** | **Current Density (A/mm$^2$)** |
|---|---|---|---|---|
| 0.160 | 0.208 | −0.814 | 0.810 | 20.577 |
| 0.211 | 0.263 | −0.814 | 0.810 | 17.503 |
| 0.267 | 0.323 | −0.814 | 0.810 | 14.964 |
| 0.326 | 0.387 | −0.814 | 0.810 | 12.855 |
| 0.390 | 0.456 | −0.814 | 0.810 | 10.989 |
| 1.200 | 2.000 | −2.017 | 1.378 | 19.098 |
| 1.200 | 1.791 | 1.378 | 2.198 | 21.103 |
| 1.200 | 1.230 | 4.581 | 6.214 | 43.579 |
| 1.200 | 1.251 | 6.340 | 6.563 | 43.249 |
| 1.200 | 1.238 | 6.615 | 7.179 | 43.643 |
| 1.200 | 1.235 | 7.258 | 9.402 | 43.332 |
| 1.200 | 1.360 | 9.520 | 9.670 | 42.882 |
| 1.000 | 1.160 | 10.330 | 10.480 | 42.882 |
| 1.000 | 1.035 | 10.630 | 14.400 | 42.882 |
| 1.000 | 1.160 | 14.550 | 14.700 | 42.882 |
| 1.000 | 1.160 | 15.330 | 15.480 | 42.882 |
| 1.000 | 1.035 | 15.630 | 19.430 | 42.882 |
| 1.000 | 1.160 | 19.580 | 20.180 | 42.882 |

Table 3: Front End Parameters

| | Length (m) | RF Frequencies (MHz) | RF Gradients (MV/m) |
|---|---|---|---|
| Drift | 57 | | |
| Buncher | 21 | 490→365 | 0→15 |
| Rotator | 24 | 364→326 | 20 |
| Cooler | 80 | 325 | 25 |

dependent optimal compromise parameters should be chosen. Large numbers of pions are lost on the beam pipe, with a greater fractional loss for higher energy pions (see Fig. 4, and note that the pion loss far exceeds the muon gain in Fig. 5). Thus a higher solenoid field downstream (giving a smaller beam size) will lead to more particles transmitted and ultimately captured (consistent with results in [1]), but the capture system will need to be retuned for a higher energy range to make optimal use of the increased field. Finally, we have inconclusive evidence that a small amount of absorber at large radius may increase the number of particles in the low energy portion of the spectrum, potentially leading to improved performance.

## CAPTURE AND COOLING SYSTEM

The 325 MHz MAP front end used for neutrino factory and muon collider scenarios [8] is used as the capture system for the present study. A schematic of that system is shown

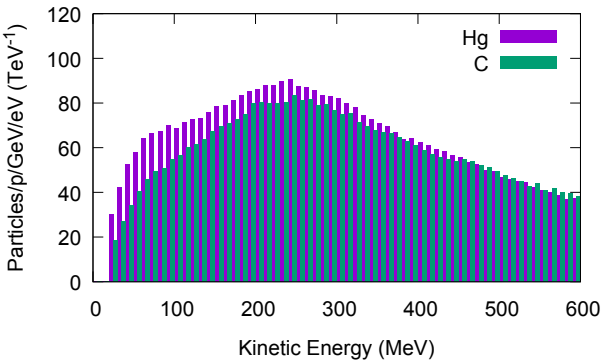


Figure 2: Distribution of positive pions 2 m downstream from the beam-target crossing point for a mercury target with an 8 GeV incident proton beam and a carbon target with a 6.75 GeV incident proton beam.

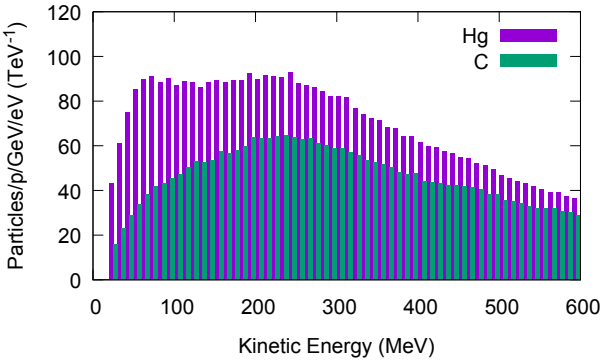


Figure 3: As in Fig. 2, but for negative pions.

in Fig. 6 and parameters of the system displayed in Table 3. The system is designed to capture muons into trains of 325 MHz bunches at a momentum of 250 MeV/$c$.

Once the beam is in the constant 2.0 T solenoid field (see above), the pions decay into muons, and the beam develops a time-energy correlation with a high-energy "head" and a low-energy "tail." Then the beam is bunched into a string of bunches in a "buncher" followed by a "phi-E" rotator section that aligns the muon bunches to nearly equal ener-

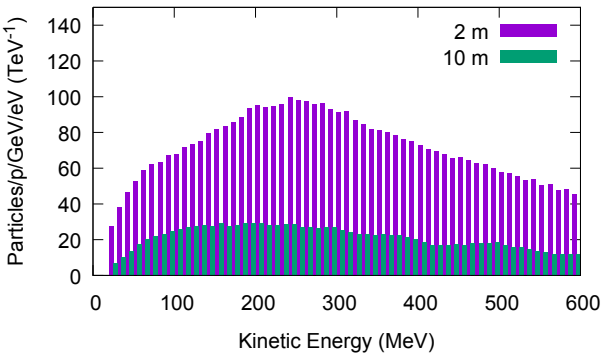


Figure 4: Positive pion spectra for a carbon target at two positions downstream from the beam-target crossing point.

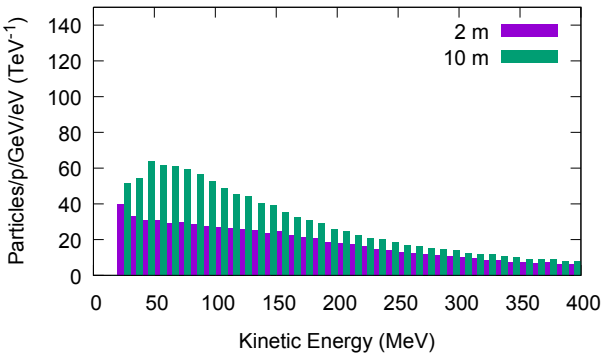


Figure 5: Positive muon spectra for a carbon target at two positions downstream from the beam-target crossing point.

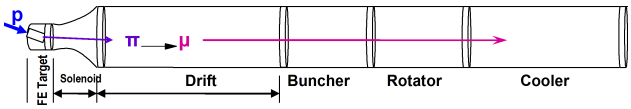


Figure 6: Schematic of the muon capture channel.

gies (matched to 325 MHz spacing) [9] and then cooled in 325 MHz cooling channel with LiH absorbers.

## SIMULATION STUDIES

We follow the muon beam down the channel, and count the number of $\mu$'s within the amplitudes $A_T < 0.03$ m, $A_L < 0.2$ m [10]; actual acceptances will depend on complete facility designs but should scale with this case. Results are shown in Fig. 7.

For the Hg target, the maximum transmission per proton per GeV of proton kinetic energy within the acceptances is $9.5 \times 10^{-3}$ $\mu^+$/p/GeV and $11.0 \times 10^{-3}$ $\mu^-$/p/GeV. For the C target, the maximum transmissions are $9.1 \times 10^{-3}$ $\mu^+$/p/GeV and $7.1 \times 10^{-3}$ $\mu^-$/p/GeV. Thus the Hg target is a bit more efficient in producing $\mu^+$, and a lot more efficient in producing $\mu^-$. This is in part due to the larger number of neutrons in Hg, which enhances $\pi^-$ production.

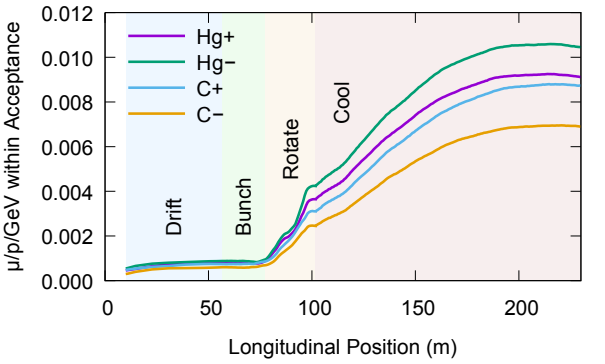


Figure 7: Muons meeting the acceptance criterion of $A_T < 30$ mm and $A_L < 200$ mm, as a function of longitudinal position, for both Hg and C targets, and both signs of muons. Values are divided by proton beam energy in GeV.

## CONCLUSION

A muon source can be generated from 6–8 GeV proton beam on either a heavy metal (Hg) or lighter element (C) target. $\mu^+$ production efficiency is similar but $\mu^-$ is more efficiently produced with a heavy metal target.

## REFERENCES


[1] Hisham Kamal Sayed and J. Scott Berg. "Optimized Capture Section for a Muon Accelerator Front End." In: *Physical Review Special Topics — Accelerators and Beams* 17 (July 28, 2014), p. 070102. DOI: 10.1103/PhysRevSTAB.17.070102.

[2] Nikolai V. Mokhov. *The MARS Code System User's Guide Version 13(95)*. Physics Note FERMILAB-FN-628. Fermilab, Apr. 1995; O. E. Krivosheev and N. V. Mokhov. "Status of MARS Electromagnetic Physics." In: *Advanced Monte Carlo for Radiation Physics, Particle Transport Simulation and Applications. Proceedings of the Monte Carlo 2000 Conference, Lisbon, 23–26 October 2000*. Ed. by A. Kling et al. Fermilab Preprint FERILAB-Conf-00/181. Berlin and Heidelberg: Springer-Verlag, 2001, pp. 141–146. DOI: 10.1007/978-3-642-18211-2_24; Nikolai V. Mokhov. *Status of MARS Code*. Preprint FERMILAB-Conf-03/053. Fermilab, Mar. 24, 2003; N. V. Mokhov et al. "Recent Enhancements to the MARS15 Code." In: *Radiation Protection Dosimetry* 116.1–4 (2005). Fermilab Preprint FERMILAB-Conf-04/053-AD, pp. 99–103. DOI: 10.1093/rpd/nci106. arXiv: nucl-th/0404084; Nikolai Mokhov. *MARS Code System*. Mar. 22, 2013. http://www-ap.fnal.gov/MARS/

[3] Nikolai V. Mokhov and Catherine C. James. *The MARS Code System User's Guide. Version 15(2014)*. May 8, 2014. http://www-ap.fnal.gov/MARS/

[4] X. Ding et al. "Optimization of a Mercury Jet Target for a Neutrino Factory or a Muon Collider." In: *Physical Review Special Topics — Accelerators and Beams* 14 (Nov. 9, 2011), p. 111002. DOI: 10.1103/PhysRevSTAB.14.111002.

[5] X. Ding et al. "Gallium as a Possible Target Material for a Muon Collider or Neutrino Factory." In: *Proceedings of IPAC2012, New Orleans, Louisiana, USA*. IPAC'12 OC and IEEE, July 2012, pp. 232–234. http://jacow.org/

[6] X. Ding, H. G. Kirk, and K. T. McDonald. "Carbon Target Optimization for a Muon Collider/Neutrino Factory with a 6.75 GeV Proton Driver." In: *Proceedings of IPAC2014, Dresden, Germany*. Ed. by Christine Petit-Jean-Genaz et al. July 2014, pp. 3982–3984. http://jacow.org/

[7] R. J. Weggel et al. "Magnet Design for the Target System of a Muon Collider/Neutrino Factory." In: *Proceedings of IPAC2014, Dresden, Germany*. Ed. by Christine Petit-Jean-Genaz et al. July 2014, pp. 3976–3978. http://jacow.org/

[8] David Neuffer and Cary Yoshikawa. "Use of 325 MHz RF in the Front End." MAP-doc-4355. Feb. 27, 2013. http://map-docdb.fnal.gov/

[9] D. Neuffer. "Exploration of the "High-Frequency" Buncher Concept." NFMCC-doc-269. Feb. 10, 2003. http://nfmcc-docdb.fnal.gov/

[10] R. C. Fernow. "Physics Analysis Performed by ECALC9." NFMCC-doc-280. Sept. 30, 2003. http://nfmcc-docdb.fnal.gov/